Excitation of low-lying collective states in ^{40}Ca and ^{208}Pb by inelastic neutron scattering

D. E. Bainum, R. W. Finlay, J. Rapaport, and J. D. Carlson*
Department of Physics, Ohio University, † Athens, Ohio 45701

W. G. Love‡
Department of Physics, University of Georgia, § Athens, Georgia 30602
and Oak Ridge National Laboratory, Oak Ridge, Tennessee 37830

(Received 9 May 1977)

Differential cross sections for elastic and inelastic scattering of neutrons from ^{208}Pb and ^{40}Ca targets have been measured at 11, 20, and 25.7 MeV incident energies. The elastic scattering data were used to provide optical model parameters for use in macroscopic and microscopic model analyses of the data using the distorted wave method. The macroscopic model analysis resulted in deformation parameters consistent with those obtained in analogous (p,p') reactions which excite the 3^- and 5^- collective states in these nuclei. The macroscopic model provides a good description of the differential cross sections. The microscopic model analysis used random-phase approximation detailed wave vectors for the states involved. Two "realistic" effective interactions were studied, one with and one without density dependence. The imaginary contribution to the effective interaction was found to be important in reproducing the shape of the differential cross section in ^{40}Ca. Exchange amplitudes were calculated exactly. The magnitudes of the 3^- cross sections for both nuclei were well described by these calculations.

[NUCLEAR REACTIONS ^{208}Pb(n,n) and (n,n'), E_n=11 and 25.7 MeV, Ca(n,n) and (n,n'), E_n=11 and 20 MeV. Measured $\sigma(\theta)$. Distorted wave analysis.]

I. INTRODUCTION

The accumulation of high quality (p, p') data[1-4] during roughly the past decade has served both to test and improve our understanding of the mechanisms by which nuclei are inelastically excited. In particular, such measurements have served to stimulate developments in the microscopic description of inelastic scattering over the past several years. Currently there exists a number of "realistic" effective interactions, based on the nucleon-nucleon force, which when used with detailed transition densities, provide an essentially parameter-free description of the differential cross sections for inelastic proton scattering.

With a few isolated exceptions, the microscopic theory has not been tested on data from (n, n') experiments. This is due to the shortage of high resolution (n, n') data, particularly on targets of separated isotopes. Since one of the primary objectives of this group is to compare (n, n') and (p, p') data[5] from nuclei with $N \neq Z$ (in particular simple shell model transitions) it was felt necessary to first compare (n, n') with (p, p') for those transitions believed to be well described both microscopically and macroscopically. At present this restricts one to the strong collective and usually isoscalar transitions. Although one expects comparable success in describing both (p, p') and (n, n') data for such nuclei, any differences should help calibrate our "resolution" for interpreting any differences we may find between (p, p') and (n, n') when exciting more "simple" (noncollective) states.

One apparent anomaly has already been reported (but see Sec. V). In particular, realistic microscopic calculations[6] overestimate the (n, n') cross section measurements of Stelson *et al.*[7] by roughly a factor of 2. Analogous calculations for protons (at a somewhat higher energy) yield very satisfactory agreement with experiment.

Apart from the considerations above, a study of the (n, n') reaction should be interesting in its own right. Although for purely isoscalar transitions (apart from Coulomb excitation) the same part of the nucleon-nucleon force should be sampled in the (p, p') and (n, n') reactions, the incident and exit particles move in different potentials. In particular, the absence of the Coulomb barrier should render neutrons more sensitive to the interior portions of the form factor and hence to any density dependence of the two-body interaction.

Thus measurements were made at Ohio University of (n, n') differential cross sections for states generally used to compare the microscopic and macroscopic formalisms to (p, p') measurements. For ^{208}Pb we obtained data for the 3^- (E_x = 2.615 MeV) and 5^- (E_x = 3.198 MeV) states at incident neutron energies of 11 and 25.7 MeV. For ^{40}Ca we obtained data at an incident energy of 11 and 20 MeV for the 3^- (E_x = 3.737 MeV) state, and at 11 MeV for the 5^- (E_x = 4.492 MeV) state. Partial

angular distributions were obtained for the 2^+ state in 2^+ ^{40}Ca at $E_x = 3.900$ MeV, and for the 5^- ($E_x = 3.09$ MeV) and ($E_x = 4.086$ MeV) states of ^{208}Pb at $E_n = 11$ MeV. This latter 2^+ state was not resolved from adjacent states, but it provided the largest yield to the peak whose partial angular distribution was extracted. At several angles the 4^-, $Q = -3.475$ MeV state was barely visible above the background in the difference spectrum resulting from subtracting the sample-out spectrum from the sample-in spectrum. This provides some hope that future (n, n') measurements may be used to study states dominated by only one or two shell model configurations. The data from this experiment are available upon request.

II. EXPERIMENTAL METHODS AND CONDITIONS

The measurements were made using the Ohio University T-11 tandem Van de Graaff accelerator and a pulsed-beam time-of-flight (TOF) spectrometer. Neutrons were produced by means of the ^{3}H$(d, n)^4$He and ^{2}H$(d, n)^3$He reactions using gas targets which were variations of the previously reported design.[8] The incident deuteron beam was pulsed and bunched at a 5 MHz repetition rate with a typical burst duration of less than 600 ps full width at half maximum (FWHM) for time-averaged beam currents up to approximately 2 μA.

The scattering samples were right circular cylinders 2 cm in diameter and 2 cm in height, and were suspended by fine threads at a distance of about 12 cm from the end of the gas cell. The ^{208}Pb sample contained 67 g of metallic Pb enriched to 99.75% of the isotope ^{208}Pb. The Ca sample consisted of 12 g of natural calcium (96.97% ^{40}Ca).

Inelastic and elastic neutron scattering data were taken in 5° intervals from 15° to 120°, and the elastic scattering angular distribution was measured to 150°. The 15° to 35° data were taken with an 8.43 m (9.92 m) flight path for the 25.7 (11.0) MeV data while the remaining data were taken with a 6.40 m flight path. The time resolution (FWHM) of the neutron elastic scattering peak

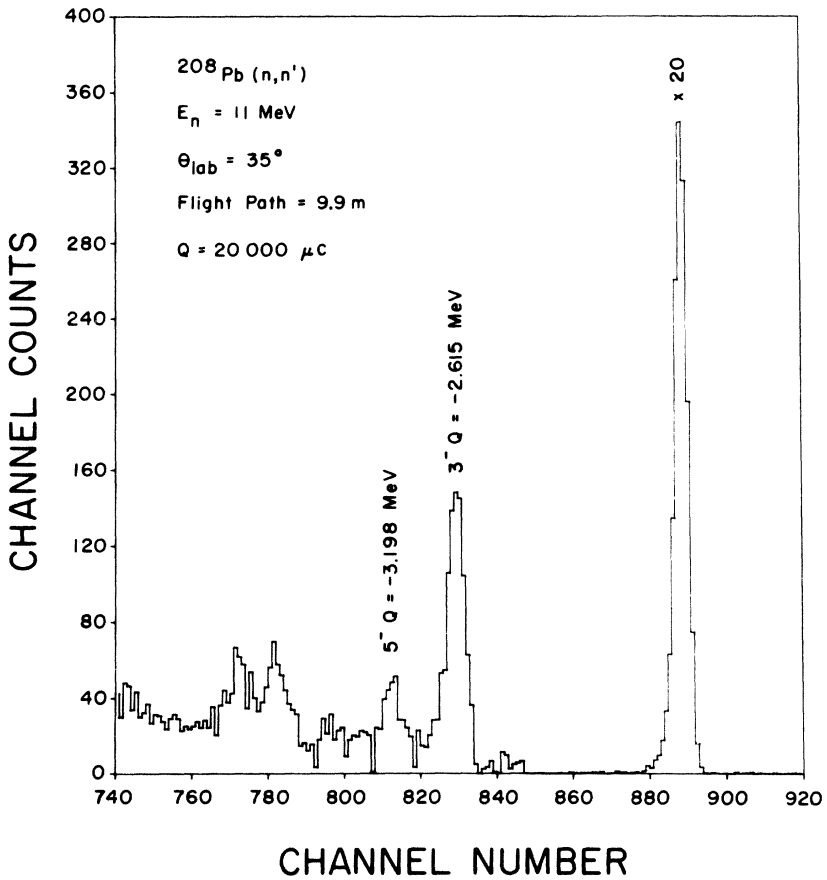

FIG. 1. Neutron time-of-flight spectrum for the ^{208}Pb(n,n') reaction. The ordinate (abscissa) denotes the counts per channel (channel numbers).

in the TOF spectrum was about 2 (1.35) ns for the 11.0 (25.7) MeV data. These time resolutions gave energy resolutions of 200 and 300 keV for the long and short flight paths at 11 MeV and 580 and 790 keV for the long and short flight paths at 25.7 MeV. The 20 MeV Ca(n, n') data were taken with a 6.62 m flight path with about 700 keV energy resolution.

The 25.7 MeV data were taken with a high efficiency detector which was developed for use with neutrons of over 20 MeV kinetic energy.[9] This detector is about five times as efficient as a "Colorado" style[10] for neutrons whose kinetic energy exceeds 20 MeV, and it has a comparable time resolution. The detector consists of 7.4 l of liquid scintillator contained in an 18.2 cm diam and 29.2 cm long acrylic tank. Photomultipliers view the front and rear scintillator faces in order to compensate for the increased time spread due to scintillator thickness. A "Colorado" style[10] detector was used for the 11 MeV data. This detector consisted of a 5.1 cm thick and 18.4 cm diam NE224 liquid scintillator mounted on an RCA 4522 photomultiplier tube. Both neutron detectors were housed in a shield made of lead and paraffin. Pulse shape discrimination was used to eliminate γ rays from the 11 MeV TOF spectrum and cosmic rays from the 25.7 MeV TOF spectrum. Figure 1 shows a typical spectrum of ^{208}Pb(n, n') at $E_n = 11.0$ MeV. A monitor detector was located at a fixed angle (−55°) relative to the zero-degree line and at a flight path of about 5 m. The monitor observed the direct output of neutrons from the gas cell.

In order to normalize the relative cross sections, the main detector was rotated to 0°, the scattering sample was removed, and the flux per monitor count which would have been incident upon the scattering sample, were it in place, was measured. With this normalization technique the absolute efficiency of the main detector does not have to be known; only the shape of the efficiency versus neutron energy need be known. This curve was measured for the "Colorado" style detector and was found to be in good agreement with a calculation made with the code DETEFF.[11]

III. DATA REDUCTION AND CORRECTIONS

The raw cross sections were corrected for the variation of the detector efficiency with energy by multiplying by (efficiency $[E_n(0°)]$)/(efficiency $[E_n(\theta)]$). This ratio was close to unity; however, for the 5$^-$, 4.492 MeV state in ^{40}Ca, this ratio was 1.17 at 15° and increased to 1.37 at 120°. The main detector was biased at 4.35 MeV neutron energy for the 11 MeV data and 15 MeV neutron energy for the 25.7 MeV data. The efficiency correction did not differ from unity by more than 1% for the 25.7 MeV data.

The data were also corrected for the anisotropy of the neutron producing reaction. The ^{2}H$(d, n)^3$He reaction was used for $E_n = 11$ MeV. If the detector, when located at zero degrees, had intercepted the same angular range in the scattering plane as did the scattering sample, then this correction need not have been made. This correction depends upon

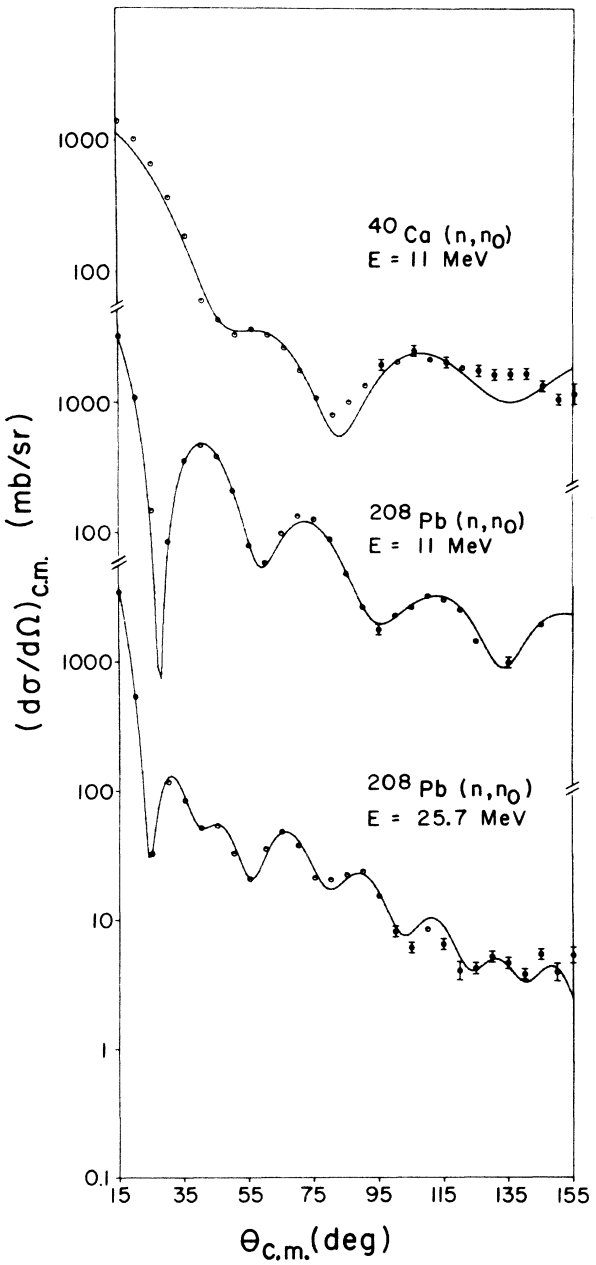

FIG. 2. Elastic differential cross sections for: Pb(n,n_0) at $E_n = 25.7$ MeV, ^{208}Pb(n,n_0) at $E_n = 11$ MeV, ^{40}Ca(n,n_0) at $E_n = 11$ MeV.

TABLE I. Optical model potentials used in this work for ^{208}Pb. The real component had a Woods-Saxon form factor while the imaginary component had a radial derivative Woods-Saxon form factor. The 25.7 MeV potential had a volume-imaginary component as well as a surface-imaginary component.

Energy (MeV)	V (MeV)	r_R (fm)	a_R (fm)	W_V (MeV)	W_D (MeV)	r_I (fm)	a_I (fm)	V_{so} (MeV)	r_{so} (fm)	a_{so} (fm)	r_{oc} (fm)	σ_{tot}^{om} (b)	σ_{tot}^{exp} (b)
11.0	43.71	1.229	0.776	•••	6.74	1.301	0.530	6.0	1.25	0.65	1.25	5.34	5.22
25.7	42.91	1.203	0.70	2.05	5.90	1.224	0.58	6.2	1.01	0.75	1.25	5.57	5.50

the diameter of the scattering sample, but was always less than 4%. The ^{3}H$(d, n)^4$He reaction was used for $E_n = 25.7$ MeV neutrons. This reaction is less anisotropic for $E_d = 9$ MeV than is the ^{2}H(d, n) reaction, so the source anisotropy correction was less than 2%.

Other corrections applied to the data were due to flux attentuation in the sample, the range of scattering angles due to the finite size of the sample, and multiple scattering within the sample. These corrections were done by a computer code MULTISCAT, which incorporates analytical and Monte Carlo methods[12] to correct the raw data for these effects.

The data for ^{40}Ca were corrected for the presence of compound nuclear processes leading to the same final states of the target. The compound nuclear angular distributions were calculated with the code HELENE[13] using the level density parameters and discrete levels used by Fu.[14] The calculated diffential cross sections were subtracted from the measured cross sections after the latter had been corrected for all previously mentioned effects.

The resulting elastic scattering angular distributions for both Ca and Pb are shown in Fig. 2. The error bars are drawn when they exceed the size of the plotting symbol, and the errors shown are due to counting statistics only. Generally, these errors were 3% for 15° to 90°, 4% for 95° to 125°, and 5% beyond that. The error in the overall normalization of the data is less than 3.5%. Also shown in Fig. 2 are the fits to the data obtained by searching on the differential cross sections using the optical model parameter search code GENOA.[15] Before the searches were done, the absolute errors in the cross sections were increased to reflect the uncertainty in the scattering angle of ±0.3°.

The resulting optical potentials for ^{208}Pb are given in Table I. The search on the 11 MeV ^{208}Pb data was begun with the potential of Fu and Perey,[16] and the search on the 25.7 MeV data was begun with the Becchetti-Greenlees neutron potential.[17] The Pb searches proceeded in three steps, varying respectively:

(1) V, W_v, W_D;
(2) V, a_R, W_v, W_D, r_1;
(3) $V, r_R, a_R, W_v, W_D, r_1, a_1$.

The strength and geometry of the spin-orbit potential were not varied. The form factor used for the volume terms was of the Woods-Saxon shape, and the surface term whose strength is W_D was taken as the radial derivative of the Woods-Saxon shape.

The search on the Ca data was begun with the geometry of van Oers[18] and only the potential strengths were varied.

IV. MACROSCOPIC MODEL ANALYSIS

Using the optical potentials determined by searching on the elastic differential cross sections, macroscopic collective model calculations were made to compare with the experimental cross sections and to extract the deformation parameters for the states excited via (n, n'). The calculations were done with the distorted wave code DWUCK.[19] The distorted waves for ^{208}Pb(n, n') were calculated with the optical potentials given in Table I. For the ^{40}Ca(n, n') calculations, the optical potentials used are reported in Table II of Ref. 20. Both real and imaginary components of the optical potential were deformed with a common deformation parameter. The value of the deformation parameter was determined for each of the final states studied by normalizing the calculations to the data.

Figure 3 shows the data with the macroscopic model fits for the 3^- (2.615 MeV) and 5^- (3.198 MeV) states of ^{208}Pb at $E_n = 11$ MeV. The collective model calculations provide a reasonably good description of the shapes of the angular distributions. The deformation parameters obtained from these calculations are given in Table II. Figure 3 also shows the data and macroscopic model calculations for these two states in ^{208}Pb at $E_n = 25.7$ MeV. The calculations are in good agreement with the data. The resulting deformation parameters are given in Table II. This table also contains the deformation lengths δ_l which are simply the products of the deformation parameters and the radii

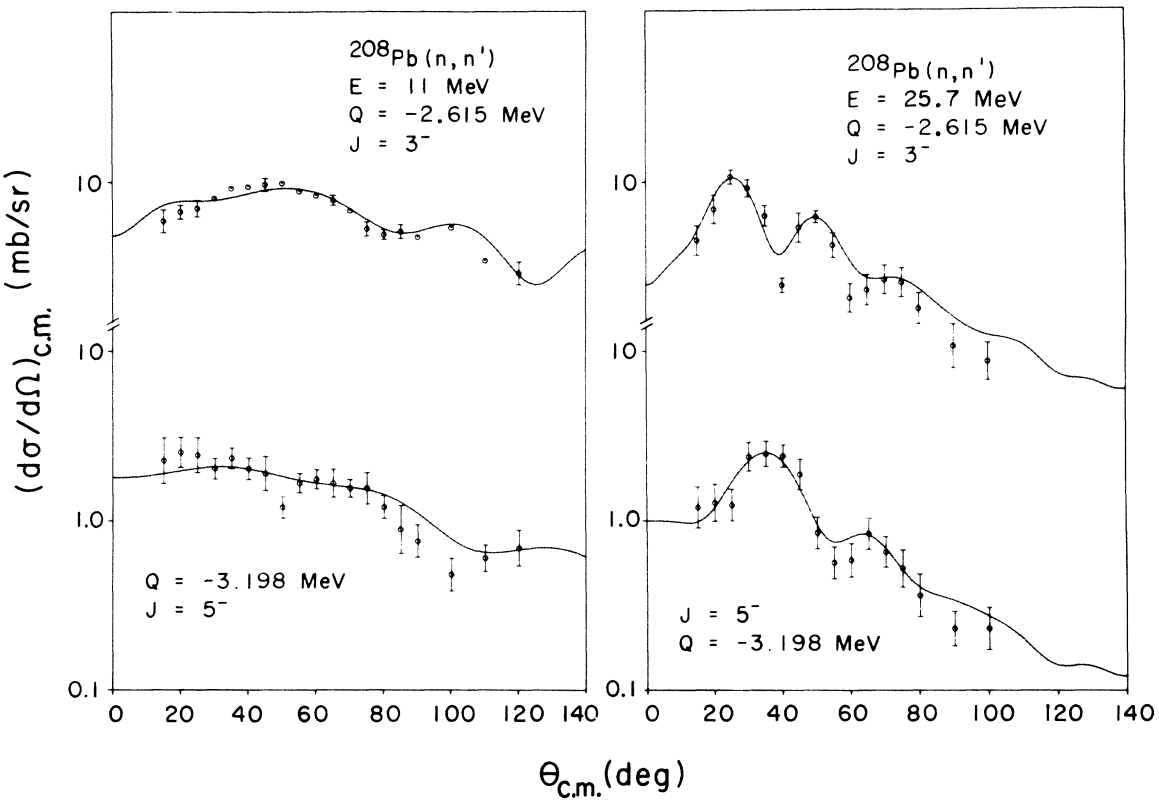

FIG. 3. Comparison between collective model calculations and experimental cross sections for ^{208}Pb(n,n').

TABLE II. Deformation parameters (β) and deformation lengths (βR_r) for states in ^{40}Ca and ^{208}Pb. The column labeled r_R gives the radius parameter of the real component of the optical potential used in the distorted wave calculations. Also shown are some values obtained with (p,p') reactions which have been reported in the literature.

Reaction	Energy (MeV)	r_R (fm)	3^-, $Q=-3.737$ MeV $\beta(3^-)$	$\beta(3^-)R_r$	2^+, $Q=-3.904$ MeV $\beta(2^+)$	$\beta(2^+)R_r$	5^-, $Q=-4.492$ MeV $\beta(5^-)$	$\beta(5^-)R_r$
^{40}Ca(n,n')	11	1.152	0.359 ± 0.021	1.41 ± 0.08	0.096 ± 0.010	0.38 ± 0.04	0.260 ± 0.039	1.02 ± 0.15
^{40}Ca(p,p')	24.9 [a]	1.16	0.354	1.40	0.106	0.42	0.230	0.91
	30.0 [a]	1.16	0.348	1.38	0.109	0.43	0.217	0.86
	34.8 [a]	1.16	0.341	1.35	0.106	0.42	0.210	0.83
	39.8 [a]	1.16	0.333	1.32	0.109	0.43	0.202	0.80
	55 [b]	1.16	0.33	1.31	•••	•••	0.17	0.67

Reaction	Energy (MeV)	r_R (fm)	3^-, $Q=-2.615$ MeV $\beta(3^-)$	$\beta(3^-)R_r$	5^-, $Q=-3.198$ MeV $\beta(5^-)$	$\beta(5^-)R_r$
^{208}Pb(n,n')	11	1.21	0.129 ± 0.007	0.93 ± 0.05	0.065 ± 0.004	0.47 ± 0.03
	25.7	1.21	0.114 ± 0.007	0.82 ± 0.05	0.064 ± 0.004	0.46 ± 0.03
^{208}Pb(p,p')	24.5 [c]	1.20	0.108	0.82	0.074	0.52
	35 [d]	1.17	0.126	0.87	0.058	0.40
	40 [e]	1.20	0.11	0.78	•••	•••
	54 [f]	1.20	0.11	0.78	0.055	0.39
	61 [g]	1.22	0.103	0.74	0.044	0.32

[a] Reference 3.
[b] Reference 21.
[c] References 22 and 25.
[d] Reference 1.
[e] Reference 23.
[f] Reference 24.
[g] Reference 25.

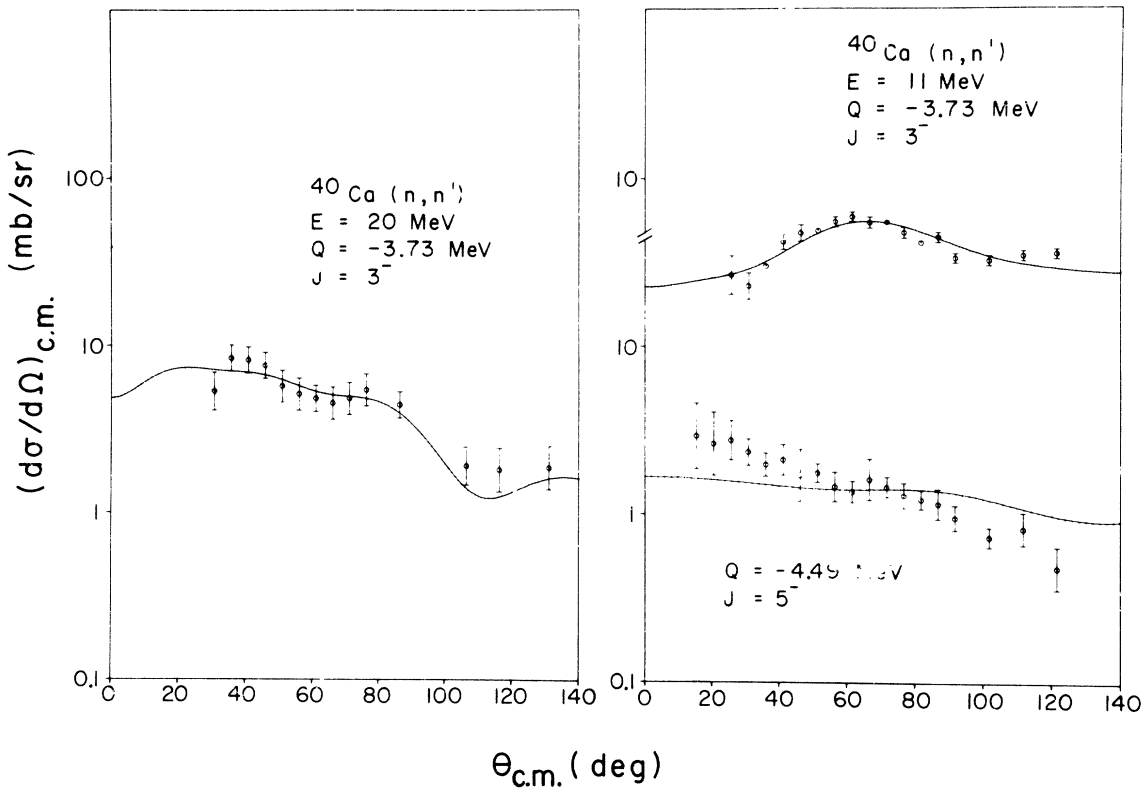

FIG. 4. Comparison between collective model calculations and experimental cross sections for ^{40}Ca(n,n').

of the *real* parts of the optical potentials. For the 3^- state β_3 (or $\delta_3 = \beta_3 R_r$) is seen (from Table II) to decrease by $\simeq 13\%$ in going from $E_n = 11$ MeV to $E_n = 25.7$ MeV. The variation is just outside the estimated errors on β_3, but is consistent with the trend in β_3 values from (p, p') measurements (apart from the earlier experiment at 24.5 MeV). The β_5 for the 5^- state exhibits essentially no energy dependence ($\simeq 2\%$) but is higher than β_5 for (p, p') at 35 MeV by $\simeq 10\%$. A number of (p, p') deformation parameters for ^{40}Ca and ^{208}Pb obtained at different proton energies are included in Table II for comparison.[1, 3, 21-25]

In Fig. 4 the data and macroscopic model calculations for the 3^- (3.737 MeV) and 5^- (4.492 MeV) states of ^{40}Ca are shown along with the macroscopic model calculations. The 3^- shape is well reproduced, but the 5^- shape has a much steeper slope than does the calculation. This may be due to the large compound nuclear corrections made to the 5^- data. For large angles these corrections were as much as 35% of the measured differential cross sections. The shape of the 5^- angular distribution before the compound nuclear corrections were made was flatter and thus more nearly reproduced by the calculation. The deformation parameters and lengths for the states observed in ^{40}Ca at $E_n = 11$ MeV are given in Table II. For excitation of the 3^- state, the value of β_3 extracted from this experiment at each neutron energy is essentially identical to that for proton scattering at $E_p = 24.9$ MeV. For the 5^- state the β_5 from (n, n') is ~13% larger than that for (p, p') at $E_p = 24.9$ MeV although the uncertainty in β_5 (~17%) is large enough for the two values to be compatible.

The 2^+ and 3^- states of ^{40}Ca were resolved only for the 15° to 35° scattering angles where the long flight path was used. The 2^+ differential cross sections for these angles were used to normalize collective model calculations with a resulting $\beta_2 = 0.096 \pm 0.010$. For the angles where the 2^+ and 3^- states were not resolved, the 2^+ differential cross section predicted by the collective mode shape was subtracted from the 3^- cross section so that the 3^- angular distribution would be due to the excitation of that state alone.

The data on which Figs. 2, 3, and 4 are based are deposited in the Physics Auxiliary Publication Service.[26]

V. MICROSCOPIC CALCULATIONS

In this section microscopic distorted wave calculations are compared with the present experimental data and with earlier[6, 25, 27, 28] results for inelastic proton scattering. The calculations were made with a modified version of the code DWBA-70[29] which includes knockon exchange amplitudes exactly.

A. Two-body effective interactions used

In the calculations reported here, attention is focused on two distinct "realistic" interactions. One of these is density independent and is based on an approximation to the G matrix calculated in ^{16}O. The result is a sum of three Yukawa terms whose small-n matrix elements approximate those of the G-matrix. We refer to this interaction as M3Y. The details are discussed in Ref. 30. The even-state interaction is based on the G matrix elements constructed from the Reid force.[30] The odd-state force is based on the matrix elements of the Sussex group.[30]

Since protons at comparable bombarding energies experience the Coulomb barrier, neutron scattering in this energy range should be relatively more sensitive to any density dependence in the effective interaction. Consequently, an alternate interaction[31] was investigated which accounts (in an approximate way) for the variation of the nuclear matter G matrix with density in a local density approximation. Such a G matrix has been approximated by a sum of three Yukawa terms, each modulated by its own characteristic function of k_F, the local Fermi momentum. The details of this interaction will be discussed elsewhere.[32] We refer to this interaction as DDD. The local density is evaluated at the position of the outermost integrand. For the direct term this is equivalent to the form-factor variable r. Since the dominant contributing ranges are 0.2 and 0.4 fm, this should be a reasonable approximation.

It should be noted that both of the above interactions have been quite successful in describing the real part of the optical potential for heavy-ion scattering.[33] This is relevant since the transitions studied here are predominantly $T = 0$.

B. ^{40}Ca(n,n')

A number[34-37] of descriptions of the low-lying odd-parity levels in ^{40}Ca have been obtained within the random-phase approximation (RPA). A comparison of these vectors is discussed in Ref. 27 for inelastic proton scattering. In the present work we use the vectors of Gillet and Sanderson[34] with the radial function determined by an oscillator parameter of $\alpha = 0.526$ fm^{-1}. With this choice of α, we find the $B(E3; 0^+ \rightarrow 3_1^-) = 1.25 \times 10^4$ fm$^6 e^2$ compared with an experimental value[38] of $(1.9 \pm 0.1) \times 10^4$ fm$^6 e^2$. Either a 7% decrease in α or a 23% increase in the proton transition density would bring the two values into agreement. Similar results[27] have been obtained using Woods-Saxon radial functions. For the 5^- state at 4.49 MeV we find the calculated $B(E5; 0^+ \rightarrow 5_1^-) = 2.10 \times 10^6$ fm$^{10} e^2$ compared to the experimental value of $(2.75 \pm 0.25) \times 10^6$ fm$^{10} e^2$. Either a 3% decrease in α or a 14% increase in the proton transition density would bring the two values into agreement.

The optical model parameters for ^{40}Ca were extracted by this group for each neutron energy and are reported elsewhere.[20] At each energy the calculations here were done using the average geometry parameters found by van Oers[18] with strengths as reported in Table II of Ref. 20.

1. 3^- state at 3.74 MeV

Figure 5 shows a comparison of experimental and theoretical differential cross sections for in-

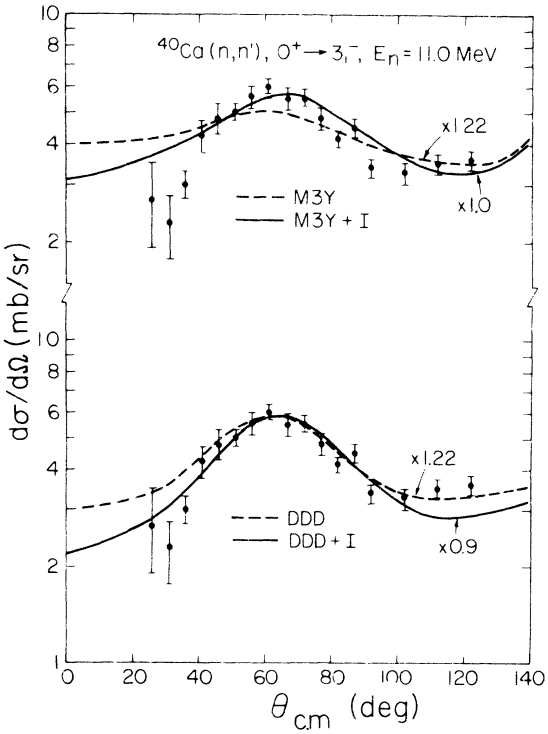

FIG. 5. Comparison of experimental and calculated (microscopic) differential cross sections for excitation of the 3_1^- state in ^{40}Ca at $E_n = 11$ MeV. M3Y (DDD) denotes a density-independent (density-dependent) interaction. I denotes the imaginary part of the collective model interaction. A renormalization factor of unity corresponds to a prediction based on the unrenormalized eigenvectors.

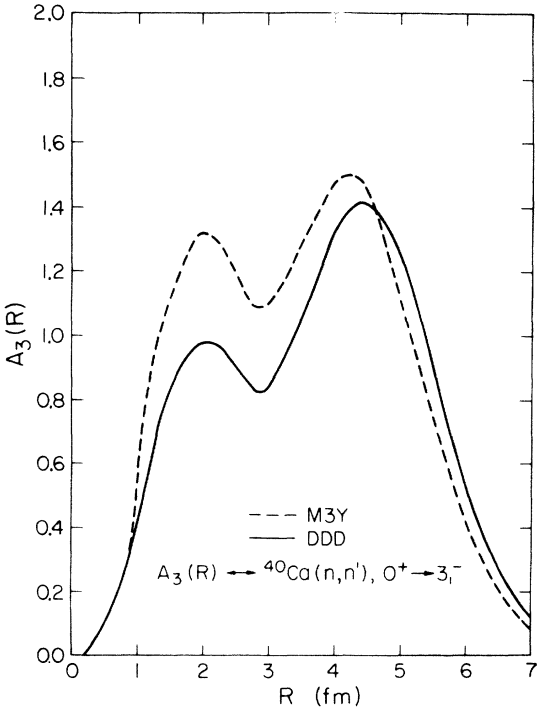

FIG. 6. Even-state microscopic form factor $A_3(r)$ for excitation of the 3_1^- level in ^{40}Ca. See Fig. 5 for legend.

cident neutrons of 11 MeV. Both the calculation using the density-independent interaction (M3Y) and that using the density-dependent interaction (DDD) are seen to require an enhancement of ~20% in cross section in order to reproduce the magnitude of the measured cross section. The (M3Y) cross section is seen to be somewhat too flat. The density dependence in the DDD calculation improves the shape of the calculated cross section near its maximum. Neither calculation represents the data well forward of ~40°. A renormalization of the 3^- transition density by 20–27% as suggested by the $B(E3)$ comparison would give too large a calculated cross section. A slight increase in the oscillator *length* accompanied by a smaller renormalization is, however, reasonable.[27]

Since the effective interaction contains, in principle, an imaginary part,[6,27] the result of including such a term as prescribed by the collective model ($\beta_3 \simeq 0.37$) is also shown in Fig. 5. As in the case of proton scattering, there is a significant improvement in the shape of the calculated angular distributions when the imaginary coupling is included. However, for $\theta_{c.m.} \lesssim 100°$ the agreement between the data and the DDD calculation is somewhat poorer. For both the density-dependent and density-independent calculations the magnitudes of the overall cross sections are reproduced within 10% when the imaginary coupling (Imf) is included. This is believed to be within the uncertainties in the calculations. Inclusion of Imf in both the M3Y and DDD calculations increases the integrated cross section by ~25%. Both the DDD and the M3Y interactions provide acceptable agreement with the data when Imf is included. In the absence of Imf, the DDD calculation is preferred.

It was anticipated that a plot of the form factor would demonstrate why the DDD calculation is preferred. However, when the odd-state forces are included, the direct form factor loses much of its usefulness since there is then very strong cancellation between the direct and exchange terms. Consequently, the odd-state force was turned off in order to examine the form factors. Figure 6 shows the resulting even-state form factors for each of the two calculations. As one might expect the DDD form factor is somewhat damped and peaks slightly further out in radius. Quantitatively, the differences are not large and this has been noted[31,33] in calculations of heavy-ion optical potentials.

Exactly analogous calculations are compared with experimental data for $E_n = 20$ MeV in Fig. 7.

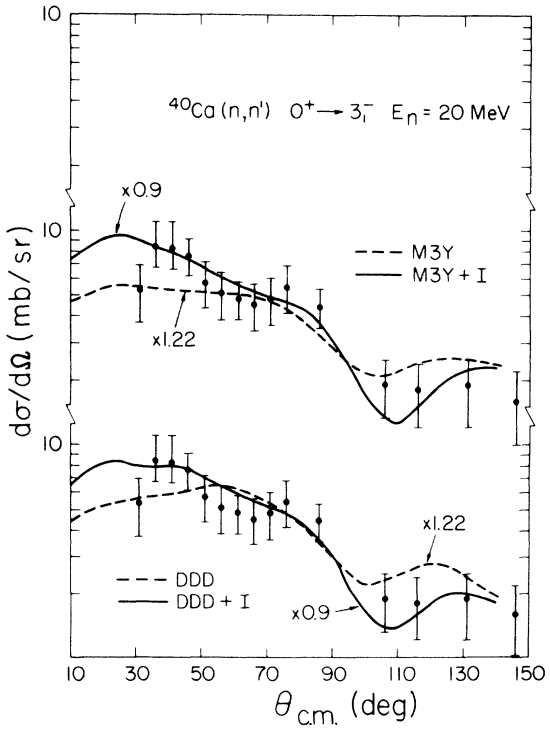

FIG. 7. Comparison of experimental and calculated (microscopic) differential cross sections for excitation of the 3_1^- level in ^{40}Ca at $E_n = 20$ MeV. See Fig. 5 for legend.

At this energy, neither the DDD nor the M3Y calculation provides an acceptable description of the shape of the experimental cross section. Just as at $E_n = 11$, MeV both calculations are too small in magnitude by ~20%. Again, inclusion of Imt provides roughly the necessary increase in the magnitude of the cross section and more importantly does so while greatly improving the agreement between the shapes of the calculated and measured cross sections. When Imt is included there is little distinction between the DDD and M3Y calculations. Both work well by microscopic model standards. As at $E_n = 11$ MeV the Imt accounts for ~25% of the integrated cross section.

2. 5^- state at 4.49 MeV

The experiment at $E_n = 11$ MeV permitted a rough extraction of the differential cross section for the 5^- state at 4.49 MeV. Figure 8 shows a comparison between the calculated and measured differential cross sections. The shape is in no way reproduced by either the M3Y or the DDD calculation. Inclusion of the noncentral parts of the force does not help. Since the collective model (surface peaked form factor) also fails to reproduce the shape of the angular distribution, no attempt was made to systematically include Imt. One purely theoretical point may be noted, however. The M3Y calculated cross section is relatively larger than the DDD result for the 5^- state compared with the 3^- state. This suggests the examination of a sequence of multipoles to test for the presence of density dependence in the interaction.

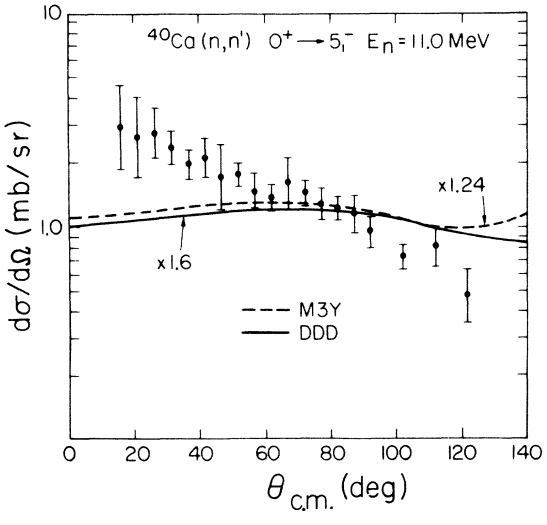

FIG. 8. Comparison between calculated (microscopic) and measured cross sections for excitation of the 5_1^- level in ^{40}Ca at $E_n = 11$ MeV. See Fig. 5 for legend.

C. ^{208}Pb(n,n')

Several calculations[39-41] have been made for the transition densities for the excitation of the lowest 3^- and 5^- states in ^{208}Pb. In Ref. 25 it is shown that the proton transition densities (ρ_p) (as inferred from electron scattering) are only qualitatively reproduced by the vectors of Refs. 39 and 40. The large-space ($3\hbar\omega$) vectors of Ring and Speth[41] (RS) are reported[6] to provide good agreement with electron scattering to the first 3^- level. All of the above densities including those taken directly from electron scattering[25] have been used to describe the inelastic excitation[6, 25, 28] of the low-lying levels in ^{208}Pb by protons between 20 and 60 MeV. Reasonable agreement with experiment is obtained for the negative-parity levels.

Reference 6 also reports calculations for the inelastic excitation of the 3^- level by 8 and 14 MeV neutrons.[7, 42] Although the excitation of this level by protons is well described by the RS vectors, calculations[6] for neutron scattering using an approximate treatment of exchange predict cross sections too large by a factor of 2. In this work we treat the knockon exchange amplitudes exactly. Moreover, Ref. 6 reports that the magnitude of the cross section for Pb(n, n') is much less sensitive to the inclusion of Imt than is proton scattering at a comparable energy. This particular result favors the examination of (n, n') versus (p, p') as a probe of the density dependence of the effective interaction.

The calculations reported here use the $3\hbar\omega$ vectors (Set $K1$) of RS[41] with an oscillator parameter $\alpha = 0.435$ fm^{-1}. With these vectors we find the calculated $B(E3; 0^+ \rightarrow 3^-) = 0.46 \times 10^6\, e^2\,\text{fm}^6$ compared with the observed value[43, 44] of $0.58 \times 10^6\, e^2\,\text{fm}^6$. This corresponds to an underestimate of ρ_p by ~12% or the necessity of a 4% reduction in the oscillator parameter α. The calculated $B(E5; 0^+ \rightarrow 5^-)$ is $2.2 \times 10^8\, e^2\,\text{fm}^{10}$ compared with a measured value[43] of $4.5 \times 10^8\, e^2\,\text{fm}^{10}$. This corresponds to an underestimate of ρ_p by ~40% or alternatively a 7% reduction in α. A more detailed discussion of the relative merits of the various RPA vectors can be found in Refs. 6, 25, and 28. The optical model parameters used in the calculations reported here are given in Table I.

1. 3^- state at 2.61 MeV

Figure 9 shows a comparison between the experimental and calculated differential cross sections $[\sigma(\theta)]$ for $E_n = 11$ and 25.7 MeV. Since Imt was found to alter the cross section by only ~10% for this transition[6] it was not included in the calculations shown here. Moreover, the large number (91) of configurations made it impractical to

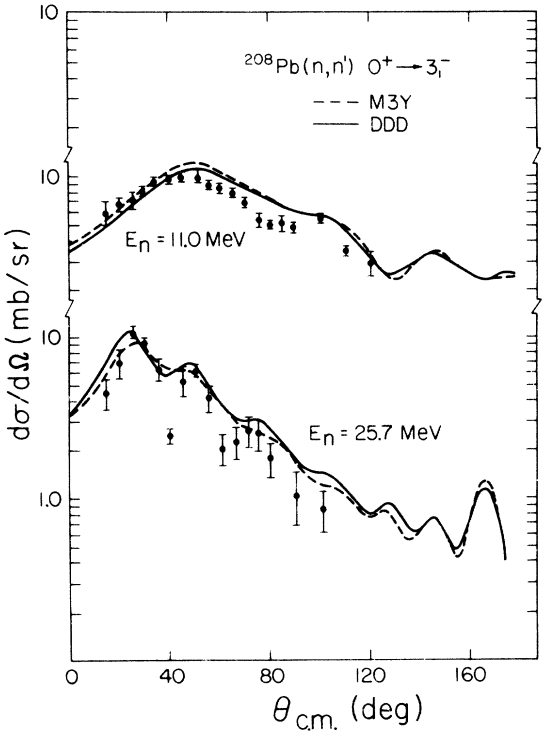

FIG. 9. Comparison of calculated (microscopic) and measured cross sections for excitation of the 3_1^- level in ^{208}Pb at E_n=11 and 25.7 MeV. See Fig. 5 for legend.

repeat the calculations. Both the M3Y and DDD calculations provide an acceptable description of both the magnitude and the shape of $\sigma(\theta)$. Analogous calculations performed with the truncated Hamada-Johnston interaction confirm that the overestimate of the (n, n') cross section found in Ref. 6 can be ascribed to the approximate treatment of the exchange terms in that article. Since both even- and odd-state forces are included in both the M3Y and DDD calculations, the ratio of the complete cross section (σ_{D+E}) to that arising from the direct term along (σ_D) ceases to be particularly useful. For example, $\sigma_{D+E}/\sigma_D \simeq 14$ at E_n=11 MeV for the M3Y force. The *net* effect of including the odd-state force in the M3Y calculation is to reduce the cross section by ~25%. Similar results hold for the DDD calculation.

2. 5^- state at 3.20 MeV

Figure 10 shows a comparison between the observed and calculated $\sigma(\theta)$ for E_n=11 and 25.7 MeV. At E_n=11 MeV the calculated $\sigma(\theta)$ appears to be slightly too small for both the M3Y and the DDD calculations which are almost identical. At E_n=25.7 MeV where the shape of $\sigma(\theta)$ is much more definitive, it is clear that the calculated cross sections are too small by ~50% with the DDD cross section being slightly larger than that using the M3Y force. This is in contrast to analogous calculations for ^{40}Ca(n, n') where the M3Y calculation yields a larger cross section relative to that of the DDD force when J^π goes from 3^- to 5^-. This is not understood. Overall, the calculated *shape* of $\sigma(\theta)$ is in very good agreement with experiment.

Also shown in Fig. 10 is the $\sigma(\theta)$ predicted by the DDD force at E_n=11 MeV enhanced by the same amount as is more clearly required at E_n=25.7 MeV. The unadjusted and renormalized $\sigma(\theta)$ are seen to roughly bracket the experimental cross section at E_n=11 MeV. The enhancement of 1.5 required of the theoretical $\sigma(\theta)$ is slightly less than the factor of 2 required to match the $B(E5)$. It is likely that a slight adjustment of α accompanied by an overall enhancement of the transition density could bring the (n, n') data in line with the $B(E5)$ result.

As in the case of the 3^- state there is little evidence in favor of a density-dependent interaction of the type considered.

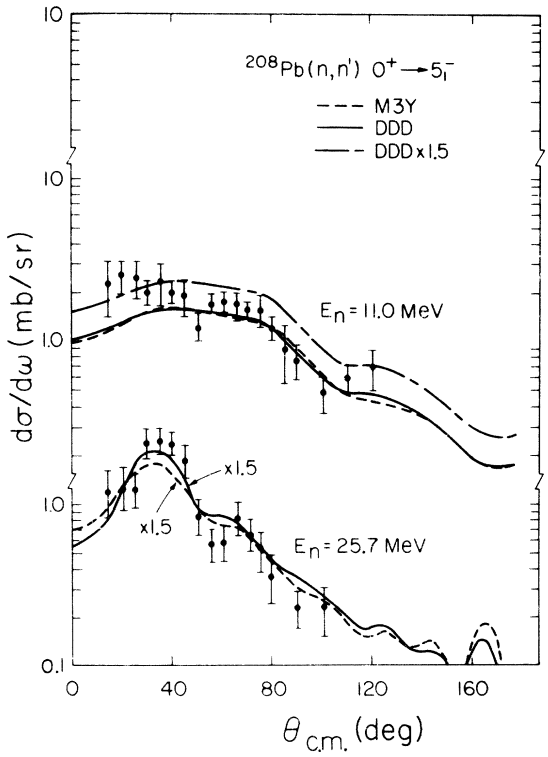

FIG. 10. Comparison of calculated (microscopic) and measured cross sections for excitation of the 5_1^- level in ^{208}Pb at E_n=11 and 25.7 MeV. See Fig. 5 for legend.

VI. DISCUSSION

With the exception of the 5^- 4.492 MeV level in ^{40}Ca, the macroscopic collective model provides a good description of the excitation of the low-lying negative-parity states in ^{40}Ca and ^{208}Pb by neutrons of 11 and ~26 MeV. In particular, the shapes of the angular distribution are well reproduced. There does exist, however, roughly a 10% difference between the β_l extracted at different neutron energies for the 3^- level in ^{208}Pb. This apparent decrease in β with increasing projectile energy is also observed in several (p, p') experiments on ^{208}Pb and is not well understood.

A comparison of ^{40}Ca(n, n') vs ^{40}Ca(p, p') at $E_n = 11$ and 20 MeV and $E_p = 24.9$ MeV yields essentially identical deformation parameters and lengths for the 3_1^- state. For the 5_1^- state in ^{40}Ca the β_l for (p, p') is smaller than that for (n, n') by ~12% which is, however, within the ~15% uncertainty in the extracted β_l.

If the comparison of β values for (p, p') and (n, n') experiments is made at equal kinetic energies inside the nucleus (i.e., at $E_n = E_p + \Delta E_{\text{Coul}}$), the deformation parameters obtained in this experiment are in very good agreement with recent proton measurements. Overall, it would appear that a definitive comparison of any differences[5] between the β_l for (p, p') and (n, n') presently requires the respective deformation parameters to differ intrinsically by at least 10%.

The microscopic calculations presented here were used to test the microscopic reaction mechanism in general and to compare two recently calculated[30-32] "realistic" interactions. For the excitation of the 3_1^- level in ^{208}Pb the microscopic calculations using the vectors of Ref. 41 are found to be in very reasonable agreement with both the magnitude and the shape of the experimental data. There is little difference between the cross sections predicted by two G-matrix effective interactions used here. One incorporates an explicit density dependence while the other does not. A stronger density dependence could of course be more readily observed. The imaginary part of the effective interaction (Imt) was not included since for ^{208}Pb(n, n') it has been reported to have only a small effect.[6] The situation for the 5_1^- level in ^{208}Pb is less satisfactory; each of the two-body interactions yields a cross section too small in magnitude by ~25–50%. This result is not too surprising since the calculated $B(E5)$ is too small by a factor of 2.

Analogous calculations for ^{40}Ca(n, n') to the 3_1^- level are found to agree (to within 10%) with the measured cross sections when Imt is included. For this case Imt is primarily essential in obtaining the correct shape of the cross section. An exception is the calculation with the density dependent force at $E_n = 11$ MeV.

A satisfactory description of the 5_1^- level in ^{40}Ca was not obtained using either the microscopic or the macroscopic model.

The anomaly found in Ref. 6 for low-energy neutron scattering has been resolved. In particular, the overestimate of the 3_1^- cross section in ^{208}Pb arose due to the approximate treatment of exchange in that article. Exchange effects can be simulated by a zero-range pseudopotential which, however, should be calibrated[45] near the bombarding energy of the data in question.

Finally, where reliable transition densities are available, a reasonable microscopic description of the experimental data emerges using either the density-independent or the density-dependent "realistic" interaction.

ACKNOWLEDGMENT

One of us (WGL) is indebted to Dr. B. Day for providing the numerical density-dependent interaction (DDD).

---

*Permanent address: Lord Corporation, Erie, Pennsylvania 16512.

†Research sponsored in part by the NSF.

‡ORAU summer faculty research participant at ORNL.

§Research sponsored in part by the NSF and by Union Carbide Corporation for the U. S. ERDA.

[1]W. T. Wagner, G. M. Crawley, G. R. Hammerstein, and H. McManus, Phys. Rev. C 12, 757 (1975), and references cited therein.

[2]J. A. Nolen, Jr. and R. J. Gleitsmann, Phys. Rev. C 11, 1159 (1975).

[3]C. R. Gruhn *et al.*, Phys. Rev. C 6, 915 (1972) and references cited therein.

[4]M. L. Whiten, A. Scott, and G. R. Satchler, Nucl. Phys. A181, 417 (1972); R. A. Hinrichs *et al.*, Phys. Rev. C 7, 1981 (1973).

[5]G. R. Satchler and W. G. Love, Nucl. Phys. A172, 449 (1971); V. A. Madsen, V. R. Brown, and J. D. Anderson, Phys. Rev. C 12, 1205 (1975).

[6]E. C. Halbert and G. R. Satchler, Nucl. Phys. A233, 265 (1974).

[7]P. H. Stelson *et al.*, Nucl. Phys. 68, 97 (1965).

[8]J. D. Carlson, Nucl. Instrum. Methods 113, 541 (1973).

[9]J. D. Carlson, R. W. Finlay, and D. E. Bainum, Nucl. Instrum. Methods (to be published).

[10]D. A. Lind *et al.*, Nucl. Instrum. Methods 130, 93 (1975).

[11]S. T. Thornton and J. R. Smith, Nucl. Instrum. Methods

96, 551 (1971).
[12]W. E. Kinney (private communication).
[13]S. K. Penny, Oak Ridge National Laboratory report No. ORNL-TM-2590, 1969 (unpublished).
[14]C. Y. Fu, At. Data Nucl. Data Tables 17, 127 (1976).
[15]F. G. Perey (private communication).
[16]C. Y. Fu and F. G. Perey, At. Data Nucl. Data Tables 16, 409 (1975).
[17]F. D. Becchetti and G. W. Greenlees, Phys. Rev. 182, 1190 (1969).
[18]W. T. H. van Oers, Phys. Rev. C 3, 1550 (1971).
[19]P. D. Kunz, University of Colorado (unpublished).
[20]J. Rapaport, J. D. Carlson, D. Bainum, T. Cheema, and R. W. Finlay, Nucl. Phys. (to be published).
[21]K. Yagi *et al.*, Phys. Lett. 10, 189 (1964).
[22]J. Saudinos *et al.*, Phys. Lett. 22, 492 (1966).
[23]M. P. Fricke and G. R. Satchler, Phys. Rev. 139, 567 (1965).
[24]M. B. Lewis, F. E. Bertrand, and C. B. Fulmer, Phys. Rev. C 7, 1966 (1973).
[25]A. Scott, N. P. Mathur, and F. Petrovich, Nucl. Phys. (to be published).
[26]See AIP document No. PAPS PRVCA-16-1377-10 for ten pages of angular distribution data on which Figs. 2, 3, and 4 of this paper are based. Order by PAPS number and journal reference from the American Institute of Physics, 335 East 45th Street, New York, N. Y. 10017. The price is $1.50 for microfiche for $5 for photocopies. This material also appears in *Current Physics Microfilm*, the monthly microfilm edition of the complete set of journals published by AIP, on frames immediately following this journal article.
[27]G. R. Satchler, Z. Phys. 260, 209 (1973).
[28]G. R. Hammerstein, R. H. Howell, and F. Petrovich, Nucl. Phys. A213, 45 (1973).
[29]R. Schaeffer and J. Raynal (unpublished).
[30]G. Bertsch, J. Borysowicz, H. McManus, and W. G. Love, Nucl. Phys. (to be published); J. P. Elliot *et al.*, Nucl. Phys. A121, 241 (1968).
[31]Y. Eisen and B. Day, Phys. Lett. 63B, 253 (1976).
[32]W. G. Love, B. Day, and G. R. Satchler (unpublished).
[33]G. R. Satchler and W. G. Love, Phys. Lett. 65B, 415 (1976).
[34]V. Gillet and E. A. Sanderson, Nucl. Phys. A91, 292 (1967).
[35]A. P. Stamp and D. F. Mayers, Nucl. Phys. 82, 296 (1966).
[36]W. J. Gerace and A. M. Green, Nucl. Phys. A113, 641 (1968).
[37]J. M. Irvine and V. F. E. Pucknell, Nucl. Phys. A173, 129 (1971).
[38]R. A. Eisenstein *et al.*, Phys. Rev. 188, 1815 (1969).
[39]V. Gillet, A. M. Green, and E. A. Sanderson, Nucl. Phys. 88, 321 (1966).
[40]T. T. S. Kuo (unpublished).
[41]P. Ring and J. Speth, Phys. Lett. 44B, 477 (1973); Nucl. Phys. A235, 315 (1974).
[42]L. Cranberg and C. D. Zafiratos, Phys. Rev. 142, 775 (1966).
[43]A. R. Barnett and W. R. Phillips, Phys. Rev. 186, 1205 (1969); M. Nagao and Y. Torizuka, Phys. Lett. 37B, 383 (1971).
[44]G. R. Satchler *et al.*, Phys. Lett. 60B, 43 (1975).
[45]W. G. Love and L. W. Owen, Nucl. Phys. A239, 74 (1975).